Stem Cell Reports
Article
ISSCR
OPEN ACCESS

Ibrutinib Displays Atrial-Specific Toxicity in Human Stem Cell-Derived Cardiomyocytes

Sanam Shafaattalab,[1,6] Eric Lin,[1] Effimia Christidi,[2] Haojun Huang,[2] Yulia Nartiss,[3] Analucia Garcia,[3] Jeehon Lee,[3] Stephanie Protze,[3,4] Gordon Keller,[3,5] Liam Brunham,[2,7] Glen F. Tibbits,[1,6,7] and Zachary Laksman[1,2,7,*]
[1]Simon Fraser University, 8888 University Drive, Burnaby, BC V5A 1A6, Canada
[2]University of British Columbia, 170-6371 Crescent Road, Vancouver, BC V6T 1Z2, Canada
[3]McEwen Stem Cell Institute, University Health Network, Toronto, ON M5G 1L7, Canada
[4]Department of Molecular Genetics, University of Toronto, Toronto, ON M5S 1A8, Canada
[5]Department of Medical Biophysics, University of Toronto, Toronto, ON M5G 1L7, Canada
[6]British Columbia Children's Hospital Research Institute, 950 West 28th Avenue, Vancouver, BC V5Z 4H4, Canada
[7]Co-senior author
*Correspondence: zlaksman@mail.ubc.ca
https://doi.org/10.1016/j.stemcr.2019.03.011

SUMMARY

Ibrutinib (IB) is an oral Bruton's tyrosine kinase (BTK) inhibitor that has demonstrated benefit in B cell cancers, but is associated with a dramatic increase in atrial fibrillation (AF). We employed cell-specific differentiation protocols and optical mapping to investigate the effects of IB and other tyrosine kinase inhibitors (TKIs) on the voltage and calcium transients of atrial and ventricular human pluripotent stem cell-derived cardiomyocytes (hPSC-CMs). IB demonstrated direct cell-specific effects on atrial hPSC-CMs that would be predicted to predispose to AF. Second-generation BTK inhibitors did not have the same effect. Furthermore, IB exposure was associated with differential chamber-specific regulation of a number of regulatory pathways including the receptor tyrosine kinase pathway, which may be implicated in the pathogenesis of AF. Our study is the first to demonstrate cell-type-specific toxicity in hPSC-derived atrial and ventricular cardiomyocytes, which reliably reproduces the clinical cardiotoxicity observed.

INTRODUCTION

Ibrutinib (IB) is an oral small-molecule irreversible inhibitor of Bruton's tyrosine kinase (BTK) that has been successfully employed in the treatment of B cell cancers. IB is first-line therapy in chronic lymphocytic leukemia (CLL) and Waldenstrom's macroglobulinemia (WM), in which it has demonstrated consistent benefit and improvement in overall survival and progression-free survival (Burger et al., 2015; Treon et al., 2015). An unexpected observation from clinical trials of IB was an increased risk of atrial fibrillation (AF), which was observed in 6%–16% of participants (Brown et al., 2017). Since continuous treatment is required to maintain clinical benefit, the cumulative incidence of AF in patients treated outside of clinical trials is likely even higher. The mechanism of IB-induced AF is unknown.

Human pluripotent stem cell-derived cardiomyocytes (hPSC-CMs) have emerged as a valuable platform for preclinical compound screening and mechanistic study of cardiotoxicity, demonstrating the unique ability to recapitulate normal and pathologic human cardiac electrophysiology and its response to drugs (Sharma et al., 2017). Most studies have focused on ventricular toxicity and employed heterogeneous populations of CMs; however, recent improvements in chamber- and cell-specific differentiation protocols have enabled the study of atrial-specific arrhythmogenic disorders such as AF (Laksman et al., 2017; Lee et al., 2017). Acquired forms of AF such as hyperthyroidism and alcohol are associated with direct effects on the unique electrophysiology of atrial CMs, including shortening of the action potential duration (APD) and an increase in the calcium (Ca^{2+}) transient duration (CaTD) (Zhang et al., 2013; Laszlo et al., 2009).

This study was designed to determine whether IB has atrial-specific cardiac electrophysiologic effects that could explain the observed association with AF. To do so, we evaluated the effects of IB on human embryonic stem cell (hESC)-derived ventricular and atrial CMs that were generated using previously published protocols (Lee et al., 2017). To investigate the arrhythmogenic potential of IB, we used optical mapping techniques to determine the drug's impact on voltage (V_m) and Ca^{2+} transients of hESC-CMs (Herron et al., 2012; Laksman et al., 2017; Lin et al., 2015), we compared IB with other structurally related tyrosine kinase inhibitors (TKIs) that have varying degrees of cardiotoxicity, including acalabrutinib, a novel experimental BTK inhibitor that has been posited to be more potent than IB with fewer off-target effects (Wu et al., 2016).

RESULTS

Phenotyping of Atrial-like and Ventricular-like hESC-CMs

We used published and optimized differentiation protocols (Dubois et al., 2011; Evseenko et al., 2010; Kataoka et al.,

This is an open access article under the CC BY-NC-ND license (http://creativecommons.org/licenses/by-nc-nd/4.0/).

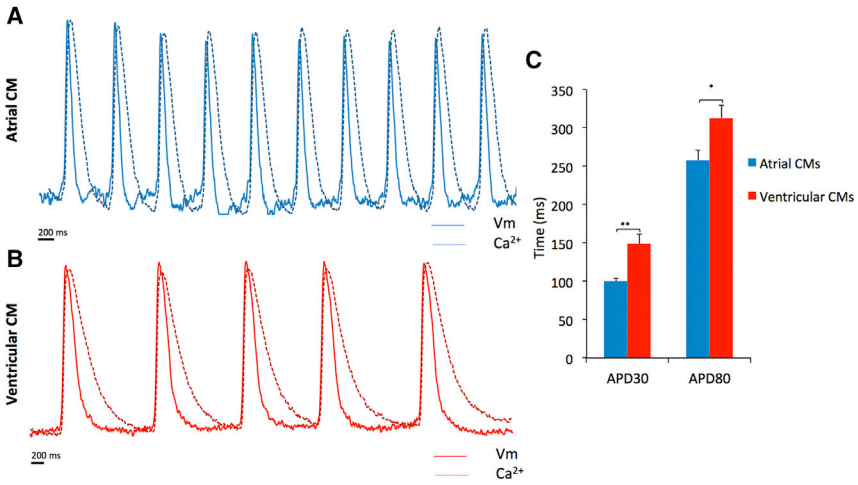

Figure 1. Characterization of Atrial and Ventricular CMs by Optical Mapping

(A) Representative spontaneously "beating" atrial CMs showing V_m (solid blue lines) and Ca^{2+} (dashed blue lines) transients.

(B) Representative spontaneously "beating" ventricular CMs showing V_m (solid red lines) and Ca^{2+} (dashed red lines) transients.

(C) Differences in action potential duration at 30% (APD_{30}, left) and 80% (APD_{80}, right) repolarization based on optical mapping of embryoid bodies paced at 60 bpm between atrial (blue) and ventricular (red) hESC-derived CMs. *$p < 0.05$; ***$p < 0.005$; n = 24 independent wells.

1997; Kattman et al., 2011; Lee et al., 2017; Prall et al., 2007) to successfully generate relatively pure populations of both atrial and ventricular CMs in two hESC lines (NKX2-5$^{egfp/w}$ and HES2). Cardiac differentiation routinely generated >80% cardiac troponin T-positive cells as determined by flow cytometry (Figure S1).

As shown in Figure 1, atrial and ventricular CMs displayed significant differences in V_m transients. The APD at 80% of repolarization (APD_{80}) (Figure 1C) was significantly ($p < 0.05$) shorter by 18% in hESC-atrial compared with ventricular cells (258 ± 13 versus 313 ± 17 ms). However, the impact of atrial phenotype on the APD was much more pronounced at APD_{30} (Figure 1C), which was shortened by 50% on the average (100 ± 4 versus 149 ± 12, $p < 0.0005$).

Impact of Acute Exposure of hESC-CMs to Ibrutinib

We exposed atrial and ventricular CMs to IB to investigate the impact of this drug on cardiac physiology to determine whether the underpinnings of arrhythmogenicity could be detected. We performed optical mapping on each sample at baseline and serially after 30 min of treatment with increasing concentrations of IB (0.1, 0.5, and 1.0 μM), a dose range chosen to reflect the half-maximal inhibitory concentration (IC_{50}) values for IB relative to BTK inhibition. In atrial CMs, IB treatment caused a significant and dose-dependent decrease in APD_{80} (Figure 2) of 8%, 26%, and 31% with IB doses of 0.1, 0.5, and 1.0 μM, respectively. Acute application of IB to atrial CMs was also associated with a dose-dependent increase in the CaTD at 80% repolarization ($CaTD_{80}$) of 8, 21, and 27% at 0.1, 0.5, and 1.0 μM, respectively. In contrast, treatment with IB had no statistically significant effect on the APD or the CaTD on ventricular CMs (Figure 2; Tables S1 and S2). These findings were replicated in atrial and ventricular CMs derived from HES2 cells (Tables S3 and S4).

Acute Impact of TKIs on hESC-CMs

To determine whether the atrial-specific effects of IB were unique to this agent, we tested the effects of six structurally related TKIs on atrial and ventricular CMs. Remarkably, none of the other TKIs tested demonstrated a significant effect on the APD of atrial CMs (Figure 3A) at any of the doses tested, suggesting that this effect is unique to IB. However, several of the TKIs resulted in significant lengthening of the $CaTD_{80}$ at the highest dose tested (Table S1). As shown in Figure 3B, all TKIs tested had significant ($p < 0.05$) lengthening effects on the $CaTD_{80}$ at a concentration of 1.0 μM, while AVL-292 was also associated with a significant and dose-dependent increase in $CaTD_{80}$ at TKI doses of 0.5 and 1.0 μM in atrial CMs.

In ventricular CMs, only nilotinib and vandetanib affected the APD_{80} and/or $CaTD_{80}$ (Figures 3C and 3D). Nilotinib caused a significant ($p < 0.05$) dose-dependent increase in APD_{80} (23%, 40%, and 52% at 0.1, 0.5, and 1.0 μM, respectively), as well as significant ($p < 0.01$) prolongation of $CaTD_{80}$, of about 2-fold at the highest concentration. Vandetanib caused a significant increase in both the APD_{80} and $CaTD_{80}$ in ventricular CMs at both 0.5 μM and 1.0 μM. Vandetanib was associated with a significant ($p < 0.05$) dose-dependent increase in APD_{80} (22%, 31%, and 41% at 0.1, 0.5, and 1.0 μM, respectively) and $CaTD_{80}$ (69% and 102% at 0.5 and 1.0 μM, respectively) in ventricular CMs. No changes to APD or CaTD were detected in DMSO control (Table S2).

The optical mapping experiments were repeated on atrial and ventricular CMs generated from the HES2 line using IB, acalabrutinib, and vandetanib (Tables S3 and S4). Only IB demonstrated a significant effect on shortening of the atrial APD, and unlike in the NKX2-5$^{egfp/w}$ line, IB was also the only agent to demonstrate prolongation of CaTD even at the highest concentrations tested. Only vandetanib was associated with a significant change in either atrial or

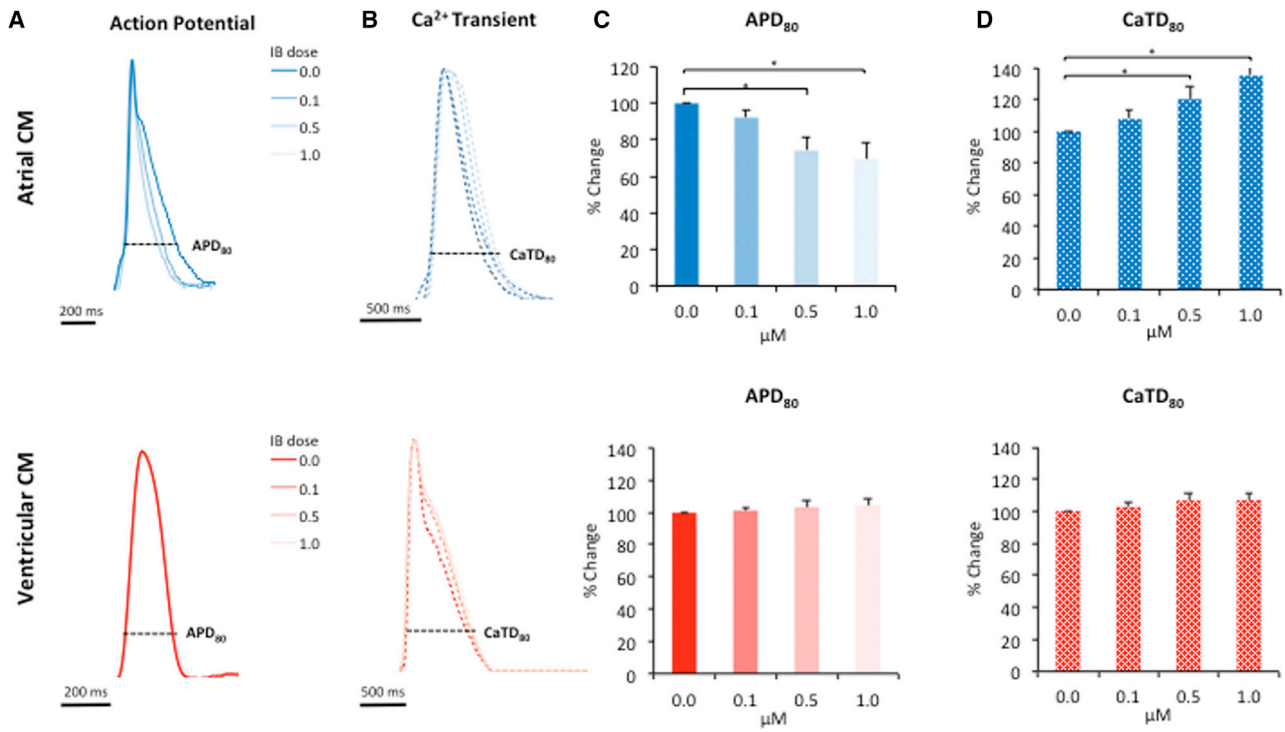

Figure 2. Simultaneous V_m and Ca^{2+} Recordings of Human Atrial and Ventricular CMs in the Presence of Ibrutinib

(A) Averaged and superimposed action potentials at three different doses of ibrutinib (IB) on atrial (blue) and ventricular (red) CMs.

(B) Averaged and superimposed Ca^{2+} transients at three doses of IB in atrial (blue) and ventricular (red) CMs.

(C) Bar graphs of the average normalized APD_{80} at three doses of IB in atrial (blue) and ventricular (red) CM. Atrial CMs demonstrated significant (*$p < 0.05$) dose-dependent shortening of APD_{80} at 0.5 and 1.0 μM ibrutinib while ventricular (red) CMs did not.

(D) $CaTD_{80}$ after exposure to IB. Atrial CMs demonstrated significant (*$p < 0.05$) dose-dependent lengthening of $CaTD_{80}$ at 0.5, and 1.0 μM ibrutinib while ventricular (red) CMs did not.

ventricular CMs with significant dose-dependent prolongation observed.

Effect of IB on Cardiac Cell Viability

We next assessed the effects of IB and acalabrutinib on cell viability in hPSC-atrial and -ventricular CMs. A reduction in cell viability is a common cellular phenotype seen in many studies of cardiotoxicity (Sharma et al., 2017). Treatment with IB led to a dose-dependent reduction in cell viability, with no apparent difference between atrial (median lethal dose [LD_{50}] = 81 μM, n = 10), and ventricular-like CMs (LD_{50} = 83 μM, n = 5) (Figure S2A). In contrast to IB, acalabrutinib resulted in less cell death in both atrial and ventricular CMs ($p < 0.0001$) (Figures S2B and S2C), consistent with the findings that acalabrutinib appears to result in a lesser degree of cardiotoxicity compared with IB.

Prolonged (72 h) and Repeated (Daily) Exposure of Atrial CMs to Ibrutinib

Since IB is prescribed chronically for patients with CLL and related disorders, we tested the effects of longer-term exposure of IB (72 h) on atrial and ventricular CMs at a dose of 0.5 μM IB by applying IB every 24 h for 3 days. The prolonged and repeated exposure of atrial CM to IB led to the appearance of delayed after-depolarizations in an alternans pattern (Figure 4). This effect was not seen in ventricular CMs at the same concentration over the same time period (data not shown).

Transcriptome Analysis of Atrial and Ventricular CMs and Cell-Specific Effects of Ibrutinib

To gain further insight into the mechanisms underlying the differential response of atrial and ventricular CMs to ibrutinib, we next performed RNA sequencing (RNA-seq) on IB- or vehicle-treated atrial and ventricular CMs. Comparing the expression of a set of candidate atrial and ventricular marker transcripts in vehicle-treated atrial and ventricular CMs, the atrial markers (*KCNA5*, *CACNA1D*, *GJA5*, *NPPA*, and *MYL7*) were expressed 3- to 182-fold higher level in atrial cells than in ventricular cells (all $p < 0.0001$), whereas ventricular markers (*MYL2*, *GJA1*, *IRX4*, *MYH7*, *HAND1*, *HEY2*, and *KCNJ2*) were upregulated 2- to

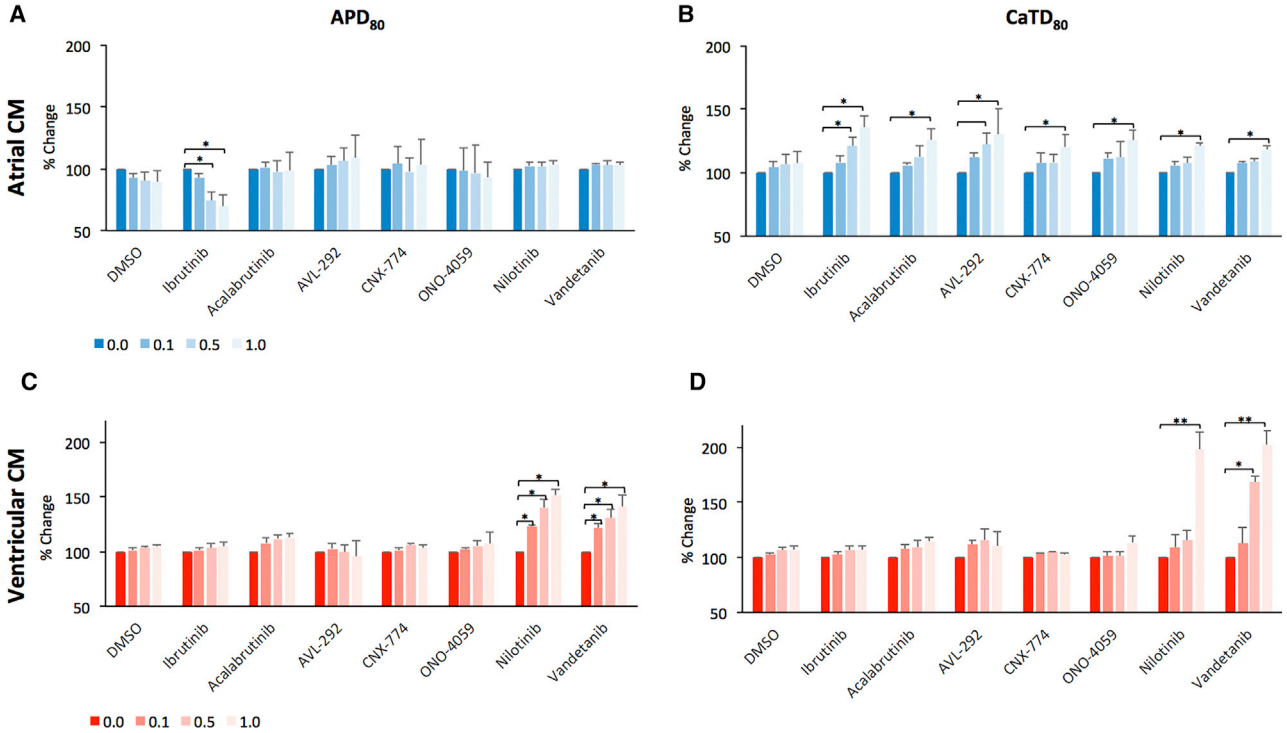

Figure 3. Effect of Six Structurally Related Tyrosine Kinase Inhibitors on the Duration of the Action Potential (APD_{80}) and the Ca^{2+} Transient ($CaTD_{80}$) in Both Atrial (Blue) and Ventricular (Red) CMs

(A and B) None of the TKIs had a significant effect on the duration of the APD_{80} in atrial CM (A). As shown in (B), all TKIs significantly prolonged the $CaTD_{80}$ at a dose of 1.0 μM in atrial CMs.

(C and D) Except for the non-BTKIs, nilotinib and vandetanib, none of the TKIs had a significant impact on either the APD_{80} or $CaTD_{80}$ in ventricular CMs. Nilotinib and vandetanib caused a significant dose-dependent lengthening of both APD_{80} (C) and $CaTD_{80}$ (D) in ventricular CMs.

*$p < 0.05$; **$p < 0.01$; n = 6 independent wells.

10-fold in ventricular cells versus atrial cells (all $p < 0.0001$), validating the chamber-specific phenotype of these cells (Figure 5A).

To compare the IB-regulated program of gene expression in atrial and ventricular CMs, we performed gene ontology enrichment analysis of all significantly differentially expressed genes between ibrutinib-treated and untreated CMs. Interestingly, the pathway that displayed the most significant differential regulation in atrial and ventricular cells was the signaling by the receptor tyrosine kinase (RTK) pathway, downregulated in atrial CMs but upregulated in ventricular CMs (Figure 5B). Most of the IB-regulated pathways were unique between atrial and ventricular CMs, with only a minority of pathways shared between the two cell types (Figure 5C). The differentially expressed genes in the RTK pathway are shown in Figure 5D. Comparing the interaction network of IB-regulated genes in this pathway between atrial and ventricular CMs reveals substantially different network patterns (Figures 5E and 5F). These data indicate that atrial and ventricular CMs respond in markedly differing ways to IB, and suggest that atrial-specific changes in RTK signaling by IB may contribute to the observed atrial-specific toxicity of this agent.

DISCUSSION

IB is a first-in-class oral BTK inhibitor, which forms a covalent bond with BTK at the cysteine-481 residue in the kinase domain, and potently blocks enzymatic activity (Patel et al., 2017). IB has known off-target effects and binds reversibly to related kinases and other proteins including epidermal growth factor receptor and the Tec family of protein-tyrosine kinases (Honigberg et al., 2010; Woyach et al., 2014). While initial efficacy was shown in patients with relapsed CLL, IB has been granted Food and Drug Administration (FDA) approval for treatment of all patients with CLL, small lymphocytic lymphoma, or WM as well as those with splenic marginal zone lymphoma or mantle cell lymphoma who have received at least one prior therapy. The clinical

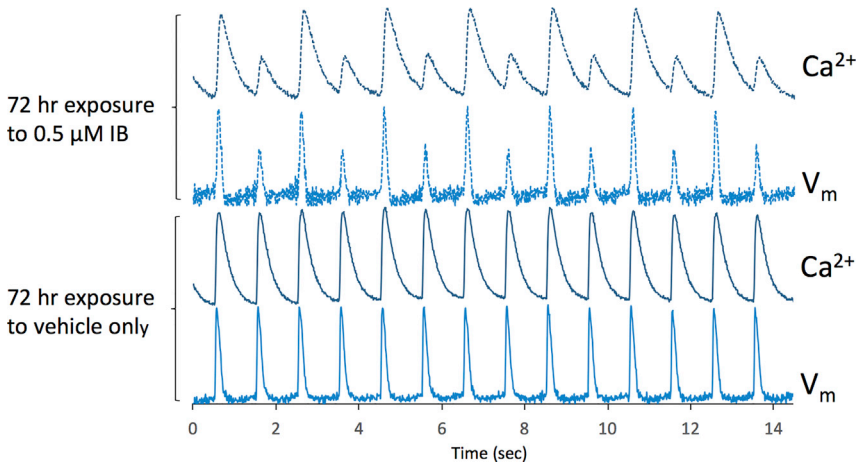

Figure 4. Effect of Prolonged (72 h) and Repeated (Daily) Exposure to 0.5 μM Ibrutinib on V_m and Ca^{2+} Transients in Atrial CMs

As can be seen in the top two traces, Ca^{2+} and V_m transients from optically mapped atrial CM exposed to ibrutinib (IB) for 72 h resulted in pronounced alternans. This effect was observed in 100% of the IB-exposed plates examined (n = 6 independent wells) and never in the vehicle-only exposure.

benefit and expanding indications likely will result in a continued increase in IB prescriptions over time (Thorp and Badoux, 2018). AF emerged as a consequence of IB administration in the first phase 3 trials, and has continued to be observed in ongoing randomized trials across a number of patient populations, with a relative risk of AF of 3.9 in patients exposed to IB (Leong et al., 2016). As IB therapy is continuous, with longer follow-up, the cumulative incidence of AF in the real world has already been shown to be higher and on the rise (Lee et al., 2016). Interestingly, IB does not appear to have a direct effect on the electrophysiology of ventricular CMs and is not associated with QT prolongation *in vivo* (de Jong et al., 2017). The mechanisms responsible for atrial arrhythmogenicity related to IB have yet to be elucidated (Thorp and Badoux, 2018).

Here we demonstrate that IB has an atrial-specific proarrhythmic effect not seen in ventricular CMs. This effect was not seen in second-generation BTK inhibitors currently in development, including acalabrutinib and ONO-4059, which have better specificity for BTK and fewer off-target effects (Jeyakumar and O'Brien, 2016). In our model system, we were able to reproduce the previous *in vitro* testing results and clinical phenotype of vandetanib and nilotinib, which are associated with acquired long QT and torsades de pointes and have cardiotoxicity-associated FDA black-box warnings. Both of these agents resulted in increased APD and CaTD when applied to ventricular CMs. The atrial and ventricular electrophysiologic effects of all TKIs tested are summarized in Table 1.

hPSC-CMs have proved to be powerful and predictive tools for the study of cardiac electrophysiology, reliably reproducing the human cardiac electrical phenotype in health, in disease, and as a model for drug screening (Colatsky et al., 2016; Kim et al., 2013; Lan et al., 2013; Moretti et al., 2010; Sun et al., 2012; Yang et al., 2015). A major step forward has been the development of differentiation protocols that promote the generation of atrial CMs that can be used to study atrial-specific diseases and drug responses (Devalla et al., 2015; Laksman et al., 2017; Lee et al., 2017). Atrial CMs are phenotypically distinct from ventricular CMs due to differential expression of multiple proteins, which result in the much shorter APDs and thus shorter refractive periods that ultimately contribute to the risk of AF (van den Berg et al., 2015; Wu et al., 2016) (Ng et al., 2008) (Elliott et al., 2011). IB has previously been studied in a mixed population of CMs, with a predominance of ventricular CMs (Blazeski et al., 2012), and was found to have a low cardiotoxicity risk relative to other TKIs. In contrast, using an atrial cell-specific model system, we show that IB has a distinct and potent cardiotoxic effect, which would be predicted to increase the risk of AF. Remarkably, the effect of IB on shortening of the APD_{80} was unique to IB and not observed with six other structurally similar TKIs. This is the first study to demonstrate the importance of evaluating drug toxicity in atrial- and ventricular-specific CM populations.

Given the known limitations of electrophysiologic screening parameters to predict AF, shorter refractory periods generally increase the propensity toward AF, and an increase in the CaTD is associated with delayed afterdepolarizations that can act as the trigger for AF initiation (Wu et al., 2016; Ng et al., 2008; Elliott et al., 2011). This was clearly demonstrated when we exposed our atrial CMs for a prolonged duration to IB, as is required clinically for ongoing therapeutic effect. The observed development of alternans would be predicted to promote atrial arrhythmias and precede AF initiation (Gong et al., 2007; Iwasaki et al., 2011; Narayan et al., 2002).

Little is known regarding the pathophysiology linking IB to an increased propensity to AF (Thorp and Badoux, 2018). Acalabrutinib, a second-generation BTK inhibitor designed to reproduce the on-target effects of IB while reducing pleiotropic effects (Byrd et al., 2016), did not demonstrate any effect on APD when applied to atrial or

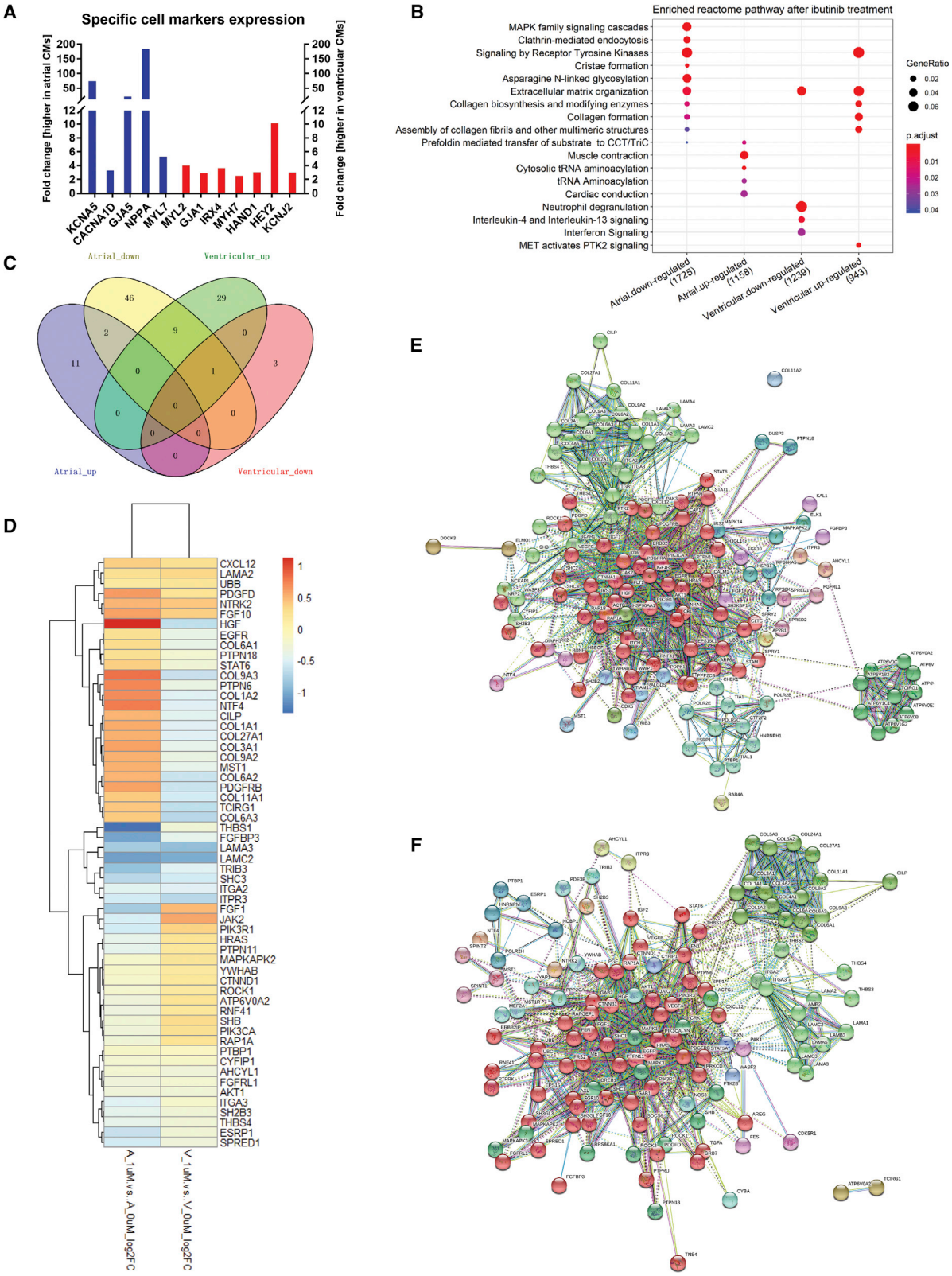

(legend on next page)

ventricular CMs (Figures 3 and 4). In cytotoxicity assays acalabrutinib was less toxic than IB, although this assay did not detect differential effects of IB on atrial and ventricular CMs. The fact that acalabrutinib and the other BTK inhibitors tested in this study target the same residue on BTK suggests that the atrial-specific pro-arrhythmic effects of IB are likely pleiotropic. IB was associated with differential chamber-specific regulation of a number of regulatory pathways including the RTK pathway, which was downregulated in atrial CMs. The RTK pathways are ubiquitous and have been implicated in AF pathogenesis in a number of complex and interrelated downstream effects on arrhythmogenesis and AF, and may be mechanistically related to the chamber-specific effects of IB (McMullen et al., 2014; Shinlapawittayatorn and Deschenes, 2010).

In conclusion, our findings indicate that cardiotoxicity screening that includes both ventricular and atrial CMs can provide improved sensitivity to detect cell-type-specific drug effects. The optical mapping platform presented here, combined with ongoing refinement and optimization of cell-specific hPSC cardiac differentiation protocols, has the potential to quickly and accurately screen for electrophysiologic cardiotoxicity at the pre-clinical stage of drug development and is uniquely suited for adaptation into high-throughput screening technologies.

EXPERIMENTAL PROCEDURES

Directed Differentiation of Atrial and Ventricular Cardiomyocytes

Culture media and differentiation of hESCs to atrial- and ventricular-like CMs employed protocols that have been reviewed previously in detail, and are available in Supplemental Information (Elliott et al., 2011; Lee et al., 2017; Ng et al., 2008). In brief, hESC NKX2-5$^{egfp/w}$ and HES2 cells were differentiated into CMs using an embryoid body (EB) protocol that employed activin A and BMP4 signaling for mesoderm induction followed by Wnt inhibition for cardiac specification. To generate atrial CMs, we added retinoic acid at the cardiac mesoderm stage (Devalla et al., 2015; Lee et al., 2017; Zhang et al., 2011). The timing and concentrations of cytokines utilized were optimized using previously described analyses (Dubois et al., 2011; Evseenko et al., 2010; Kataoka et al., 1997; Kattman et al., 2011; Prall et al., 2007). Details regarding flow cytometry can be found in Supplemental Information.

Optical Mapping

The hESC-CMs were loaded with 15 μM of the V_m-sensitive potentiometric dye RH-237 (Molecular Probes, Eugene, OR) and 5 μM of Ca^{2+}-sensitive dye Rhod-2AM (Molecular Probes). Blebbistatin, a myosin ATPase inhibitor (Sigma-Aldrich), was employed to avoid motion artifact (Fedorov et al., 2007; Lin et al., 2014). Atrial and ventricular CMs were excited by 532-nm LEDs and incubated at 37°C. RH-237 and Rhod-2 emissions were monitored using >710-nm long-pass and 565- to 600-nm bandpass filters, respectively. Both signals were captured with a single Hamamatsu ORCA Flash 4 digital sCMOS camera by incorporating an optical image splitter. Images were captured at the camera's native resolution of 2,048 × 2,048 pixels (pixel dimensions 5 μm). The TKIs (MedChem Express) were diluted in DMSO and added to the culture dish in sequentially increasing concentrations (0.1, 0.5, and 1.0 μM) at 15-min intervals. The DMSO final concentration did not exceed 0.5%. Independent differentiation runs were studied in isolated wells. Each well contained EBs that varied in shape and size, with an average diameter of 750 μm (0.5 mm^2). EBs were seeded at 85% coverage such that each image recording contained an average of 75 EBs. All EBs identified within the 5 × 10-mm image area were analyzed simultaneously (see below). Analysis algorithms were written using Interactive Data Language (Harris Geospatial). To quantify objectively the entire CM population under study in a repeatable and consistent manner, we also used whole-image analysis. This allowed for the generation of APD and CaTD maps. The histogram of the APD and CaTD maps contains the distribution, and the histogram of the difference between two recordings contains the distribution of the effect (Figure S3). In some analyses, the difference result was normalized by the magnitude of the first recording to calculate the percent effect. Further details regarding optical mapping can be found in Supplemental Information.

Drug Screening

Of the more than 20 TKIs currently approved by the FDA, a number have been associated with cardiotoxicity (Yeh and Bickford, 2009). Here we chose to look at IB and four closely related BTK

Figure 5. RNA-Seq Data from Atrial and Ventricular CMs and the Effects of Ibrutinib

(A) Atrial- and ventricular-specific gene expression profiles. Genes in red are expressed to a higher degree in atrial CMs and genes in blue are expressed to a higher degree in ventricular CMs. Adjusted p value <0.05.

(B) Enriched reactome pathways of atrial and ventricular CMs after ibrutinib treatment. Only the top-ranked pathways are shown based on the adjusted p value.

(C) Venn diagram of all enriched reactome pathways in atrial and ventricular CMs. Gene sets are divided into up- or downregulated lists in these two cell types.

(D) Heatmap of significant differentially expressed genes in both atrial and ventricular CMs after ibrutinib treatment in the pathway of signaling by receptor tyrosine kinases. Colors represent log_2-fold change value of each gene. Adjusted p value <0.05.

(E and F) Predicted protein network in the pathway of signaling by receptor tyrosine kinases after ibrutinib treatment. (E) shows 137 genes within the pathway in atrial cells and (F) shows 128 genes within the pathway in ventricular cells. Adjusted p value <0.05. Network nodes represent proteins and edges represent protein-protein associations. Nodes' colors are obtained according to Markov clustering (inflation parameter = 3). Networks were drawn using STRING.

Table 1. Summary of Atrial and Ventricular Electrophysiologic Effects of All TKIs Tested

	hESC-derived Atrial CMs		hESC-derived Ventricular CMs		
TKIs	**ΔAPD**	**ΔCaTD**	**ΔAPD**	**ΔCaTD**	**Clinically reported Cardiotoxicity**
Ibrutinib	↓↓	↑↑	↔	↔	AF
Acalabrutinib	↔	↔ ↑	↔	↔	None
AVL-292	↔	↑↑	↔	↔	None
CNX-774	↔	↔ ↑	↔	↔	None
ONO-4059	↔	↔ ↑	↔	↔	None
Nilotinib	↔	↔ ↑	↑↑	↑↑	LQT, LV, Vas
Vandetanib	↔	↔ ↑	↑↑	↑↑	LQT, TdP, SCD, HF

hESC, human embryonic stem cells; CM, cardiomyocytes; TKI, tyrosine kinase inhibitor; APD, action potential duration; CaTD, calcium transient duration; AF, atrial fibrillation; LQT, long QT syndrome; LV, decrease in left ventricular ejection fraction; Vas, vascular disorders; TdP, torsades de pointes; SCD, sudden cardiac death; HF, heart failure. Red cells: statistical significance reached. Green cells: no statistically significant difference. Split red and green cells: significant differences in only one hESC line and only at the highest concentrations tested.

inhibitors (CNX-774, ONO-4059, AVL-292, and acalabrutinib), and two additional non-BTK TKIs (nilotinib and vandetanib) in terms of their effects on atrial and ventricular CM parameters. The BTK inhibitors had similar IC_{50} values and thus were tested over the same concentrations as described in Supplemental Experimental Procedures. Among the BTK inhibitors currently available, those selected were similar in structure to IB, target the same Cys-481 residue, and are second-generation BTK inhibitors employed for similar indications (Hutchinson and Dyer, 2014; Patel et al., 2017). Nilotinib and vandetanib, the non-BTK TKIs, have well-documented cardiotoxic effects and provided a positive control for ventricular toxicity in this study (Sharma et al., 2017).

RNA Sequencing

Total RNA of hESC-CMs was isolated by Illustra RNAspin Mini Isolation Kit (GE Healthcare) after 24 h of incubation of 1 μM ibrutinib in the experimental group and vehicle (DMSO) in the control group. Each condition has three replicates. RNA quality was assessed by measuring the RNA integrity number using an Agilent 2100 Bioanalyzer (Agilent Technologies). Library preparation was performed following the standard protocol for the NEBnext Ultra II Stranded mRNA (New England Biolabs) and sequencing was performed on the NextSeq 500 (Ilumina) with 20 million paired-end reads. Reads were filtered by Bowtie against abundant sequences. Filtered reads were aligned to the reference genome UCSC hg38 using STAR aligner and read counting was performed using featureCounts. Raw counts >5 in more than two samples was set as background threshold. Read counts normalization and differential expression were analyzed in the R/Bioconductor environment using the DESeq2 package. The ClusterProfiler package was used for pathway enrichment analysis and STRING was used for protein network prediction. An adjusted p value of <0.05 was considered statistically significant. The RNA-seq data have been submitted to the GEO database and the accession number is GEO: GSE128688.

Statistical Analysis

Each well was recorded as shown in Results as 1 repeat (N). The minimum number of N performed was 5. The minimum number of differentiation batches tested for each drug was 2, with a maximum of 8 (see Supplemental Information). The results were expressed as means ± SE. Statistical significance in response to different doses of each TKI to determine the V_m and Ca^{2+} transient durations (APD and Ca^{2+} and Ca^{2+} TD, respectively) were determined using one-way ANOVA, followed by Tukey's post hoc test to determine whether there were significant differences between the means. p values of <0.05 were considered significant. The JMP 11 software package was used for all analyses.

SUPPLEMENTAL INFORMATION

Supplemental Information can be found online at https://doi.org/10.1016/j.stemcr.2019.03.011.

AUTHOR CONTRIBUTIONS

The study concept was generated by L.B., Z.L., G.K., and G.F.T. The experimentation was completed by S.S., Y.N., E.L., S.P., J.L., E.C., A.G., and H.H. with support from Z.L., G.F.T., L.B., and G.K. Analysis was completed by S.S., H.H., E.L., G.T., Z.L., E.C., and L.B. Manuscript and figure preparation by S.S., E.L., E.C., L.B., G.T., Z.L., and H.H. with input from S.P., J.L., and G.K.

ACKNOWLEDGMENTS

This study was funded in part by the Stem Cell Network to L.B., Z.L., and G.F.T. and by the Canadian Institutes of Health Research (CIHR) to G.F.T. and L.B. (PJT153118). G.F.T. was also supported as a Canada Research Chair. L.B. is a CIHR New Investigator and Michael Smith Foundation for Health Research scholar. Z.L. was supported by the Michael Smith Foundation, the Charles Kerr Scholarship, and the St. Paul's Hospital Foundation.

Received: May 12, 2018
Revised: March 26, 2019
Accepted: March 27, 2019
Published: April 25, 2019

REFERENCES

Blazeski, A., Zhu, R., Hunter, D.W., Weinberg, S.H., Boheler, K.R., Zambidis, E.T., and Tung, L. (2012). Electrophysiological and contractile function of cardiomyocytes derived from human embryonic stem cells. Prog. Biophys. Mol. Biol. *110*, 178–195.

Brown, J.R., Moslehi, J., O'Brien, S., Ghia, P., Hillmen, P., Cymbalista, F., Shanafelt, T.D., Fraser, G., Rule, S., Kipps, T.J., et al. (2017). Characterization of atrial fibrillation adverse events reported in ibrutinib randomized controlled registration trials. Haematologica *102*, 1796–1805.

Burger, J.A., Tedeschi, A., Barr, P.M., Robak, T., Owen, C., Ghia, P., Bairey, O., Hillmen, P., Bartlett, N.L., Li, J., et al. (2015). Ibrutinib as initial therapy for patients with chronic lymphocytic leukemia. N. Engl. J. Med. *373*, 2425–2437.

Byrd, J.C., Harrington, B., O'Brien, S., Jones, J.A., Schuh, A., Devereux, S., Chaves, J., Wierda, W.G., Awan, F.T., Brown, J.R., et al. (2016). Acalabrutinib (ACP-196) in relapsed chronic lymphocytic leukemia. N. Engl. J. Med. *374*, 323–332.

Colatsky, T., Fermini, B., Gintant, G., Pierson, J.B., Sager, P., Sekino, Y., Strauss, D.G., and Stockbridge, N. (2016). The comprehensive in vitro proarrhythmia assay (CiPA) initiative—update on progress. J. Pharmacol. Toxicol. Methods *81*, 15–20.

de Jong, J., Hellemans, P., Jiao, J.J., Huang, Y., Mesens, S., Sukbuntherng, J., and Ouellet, D. (2017). Ibrutinib does not prolong the corrected QT interval in healthy subjects: results from a thorough QT study. Cancer Chemother. Pharmacol. *80*, 1227–1237.

Devalla, H.D., Schwach, V., Ford, J.W., Milnes, J.T., El-Haou, S., Jackson, C., Gkatzis, K., Elliott, D.A., Chuva de Sousa Lopes, S.M., Mummery, C.L., et al. (2015). Atrial-like cardiomyocytes from human pluripotent stem cells are a robust preclinical model for assessing atrial-selective pharmacology. EMBO Mol. Med. *7*, 394–410.

Dubois, N.C., Craft, A.M., Sharma, P., Elliott, D.A., Stanley, E.G., Elefanty, A.G., Gramolini, A., and Keller, G. (2011). SIRPA is a specific cell-surface marker for isolating cardiomyocytes derived from human pluripotent stem cells. Nat. Biotechnol. *29*, 1011–1018.

Elliott, D.A., Braam, S.R., Koutsis, K., Ng, E.S., Jenny, R., Lagerqvist, E.L., Biben, C., Hatzistavrou, T., Hirst, C.E., Yu, Q.C., et al. (2011). NKX2-5(eGFP/w) hESCs for isolation of human cardiac progenitors and cardiomyocytes. Nat. Methods *8*, 1037–1040.

Evseenko, D., Zhu, Y., Schenke-Layland, K., Kuo, J., Latour, B., Ge, S., Scholes, J., Dravid, G., Li, X., MacLellan, W.R., et al. (2010). Mapping the first stages of mesoderm commitment during differentiation of human embryonic stem cells. Proc. Natl. Acad. Sci. U S A *107*, 13742–13747.

Fedorov, V.V., Lozinsky, I.T., Sosunov, E.A., Anyukhovsky, E.P., Rosen, M.R., Balke, C.W., and Efimov, I.R. (2007). Application of blebbistatin as an excitation-contraction uncoupler for electrophysiologic study of rat and rabbit hearts. Heart Rhythm *4*, 619–626.

Gong, Y., Xie, F., Stein, K.M., Garfinkel, A., Culianu, C.A., Lerman, B.B., and Christini, D.J. (2007). Mechanism underlying initiation of paroxysmal atrial flutter/atrial fibrillation by ectopic foci: a simulation study. Circulation *115*, 2094–2102.

Herron, T.J., Lee, P., and Jalife, J. (2012). Optical imaging of voltage and calcium in cardiac cells & tissues. Circ. Res. *110*, 609–623.

Honigberg, L.A., Smith, A.M., Sirisawad, M., Verner, E., Loury, D., Chang, B., Li, S., Pan, Z., Thamm, D.H., Miller, R.A., et al. (2010). The Bruton tyrosine kinase inhibitor PCI-32765 blocks B-cell activation and is efficacious in models of autoimmune disease and B-cell malignancy. Proc. Natl. Acad. Sci. U S A *107*, 13075–13080.

Hutchinson, C.V., and Dyer, M.J. (2014). Breaking good: the inexorable rise of BTK inhibitors in the treatment of chronic lymphocytic leukaemia. Br. J. Haematol. *166*, 12–22.

Iwasaki, Y.K., Nishida, K., Kato, T., and Nattel, S. (2011). Atrial fibrillation pathophysiology: implications for management. Circulation *124*, 2264–2274.

Jeyakumar, D., and O'Brien, S. (2016). The next generation of targeted molecules for the treatment of chronic lymphocytic leukemia. Oncology (Williston Park) *30*, 1008–1015.

Kataoka, H., Takakura, N., Nishikawa, S., Tsuchida, K., Kodama, H., Kunisada, T., Risau, W., Kita, T., and Nishikawa, S.I. (1997). Expressions of PDGF receptor alpha, c-Kit and Flk1 genes clustering in mouse chromosome 5 define distinct subsets of nascent mesodermal cells. Dev. Growth Differ. *39*, 729–740.

Kattman, S.J., Witty, A.D., Gagliardi, M., Dubois, N.C., Niapour, M., Hotta, A., Ellis, J., and Keller, G. (2011). Stage-specific optimization of activin/nodal and BMP signaling promotes cardiac differentiation of mouse and human pluripotent stem cell lines. Cell Stem Cell *8*, 228–240.

Kim, C., Wong, J., Wen, J., Wang, S., Wang, C., Spiering, S., Kan, N.G., Forcales, S., Puri, P.L., Leone, T.C., et al. (2013). Studying arrhythmogenic right ventricular dysplasia with patient-specific iPSCs. Nature *494*, 105–110.

Laksman, Z., Wauchop, M., Lin, E., Protze, S., Lee, J., Yang, W., Izaddoustdar, F., Shafaattalab, S., Gepstein, L., Tibbits, G.F., et al. (2017). Modeling atrial fibrillation using human embryonic stem cell-derived atrial tissue. Sci. Rep. *7*, 5268.

Lan, F., Lee, A.S., Liang, P., Sanchez-Freire, V., Nguyen, P.K., Wang, L., Han, L., Yen, M., Wang, Y., Sun, N., et al. (2013). Abnormal calcium handling properties underlie familial hypertrophic cardiomyopathy pathology in patient-specific induced pluripotent stem cells. Cell Stem Cell *12*, 101–113.

Laszlo, R., Eick, C., Schwiebert, M., Schreiner, B., Weig, H.J., Weretka, S., Bosch, R.F., and Schreieck, J. (2009). Alcohol-induced electrical remodeling: effects of sustained short-term ethanol infusion on ion currents in rabbit atrium. Alcohol Clin. Exp. Res. *33*, 1697–1703.

Lee, H.J., Chihara, D., Wang, M., Mouhayar, E., and Kim, P. (2016). Ibrutinib-related atrial fibrillation in patients with mantle cell lymphoma. Leuk. Lymphoma *57*, 2914–2916.

Lee, J.H., Protze, S.I., Laksman, Z., Backx, P.H., and Keller, G.M. (2017). Human pluripotent stem cell-derived atrial and ventricular cardiomyocytes develop from distinct mesoderm populations. Cell Stem Cell *21*, 179–194.e4.

Leong, D.P., Caron, F., Hillis, C., Duan, A., Healey, J.S., Fraser, G., and Siegal, D. (2016). The risk of atrial fibrillation with ibrutinib use: a systematic review and meta-analysis. Blood *128*, 138–140.

Lin, E., Craig, C., Lamothe, M., Sarunic, M.V., Beg, M.F., and Tibbits, G.F. (2015). Construction and use of a zebrafish heart voltage and calcium optical mapping system, with integrated electrocardiogram and programmable electrical stimulation. Am. J. Physiol. Regul. Integr. Comp. Physiol. *308*, R755–R768.

Lin, E., Ribeiro, A., Ding, W., Hove-Madsen, L., Sarunic, M.V., Beg, M.F., and Tibbits, G.F. (2014). Optical mapping of the electrical activity of isolated adult zebrafish hearts: acute effects of temperature. Am. J. Physiol. Regul. Integr. Comp. Physiol. *306*, R823–R836.

McMullen, J.R., Boey, E.J., Ooi, J.Y., Seymour, J.F., Keating, M.J., and Tam, C.S. (2014). Ibrutinib increases the risk of atrial fibrillation, potentially through inhibition of cardiac PI3K-Akt signaling. Blood *124*, 3829–3830.

Moretti, A., Bellin, M., Welling, A., Jung, C.B., Lam, J.T., Bott-Flugel, L., Dorn, T., Goedel, A., Hohnke, C., Hofmann, F., et al. (2010). Patient-specific induced pluripotent stem-cell models for long-QT syndrome. N. Engl. J. Med. *363*, 1397–1409.

Narayan, S.M., Bode, F., Karasik, P.L., and Franz, M.R. (2002). Alternans of atrial action potentials during atrial flutter as a precursor to atrial fibrillation. Circulation *106*, 1968–1973.

Ng, E.S., Davis, R., Stanley, E.G., and Elefanty, A.G. (2008). A protocol describing the use of a recombinant protein-based, animal product-free medium (APEL) for human embryonic stem cell differentiation as spin embryoid bodies. Nat. Protoc. *3*, 768–776.

Patel, V., Balakrishnan, K., Bibikova, E., Ayres, M., Keating, M.J., Wierda, W.G., and Gandhi, V. (2017). Comparison of acalabrutinib, a selective Bruton tyrosine kinase inhibitor, with ibrutinib in chronic lymphocytic leukemia cells. Clin. Cancer Res. *23*, 3734–3743.

Prall, O.W., Menon, M.K., Solloway, M.J., Watanabe, Y., Zaffran, S., Bajolle, F., Biben, C., McBride, J.J., Robertson, B.R., Chaulet, H., et al. (2007). An Nkx2-5/Bmp2/Smad1 negative feedback loop controls heart progenitor specification and proliferation. Cell *128*, 947–959.

Sharma, A., Burridge, P.W., McKeithan, W.L., Serrano, R., Shukla, P., Sayed, N., Churko, J.M., Kitani, T., Wu, H., Holmstrom, A., et al. (2017). High-throughput screening of tyrosine kinase inhibitor cardiotoxicity with human induced pluripotent stem cells. Sci. Transl. Med. *9*. https://doi.org/10.1126/scitranslmed.aaf2584.

Shinlapawittayatorn, K., and Deschenes, I. (2010). Alteration of tyrosine kinase signaling: another player in the arrhythmogenesis of atrial fibrillation? Heart Rhythm *7*, 1253–1254.

Sun, N., Yazawa, M., Liu, J., Han, L., Sanchez-Freire, V., Abilez, O.J., Navarrete, E.G., Hu, S., Wang, L., Lee, A., et al. (2012). Patient-specific induced pluripotent stem cells as a model for familial dilated cardiomyopathy. Sci. Transl. Med. *4*, 130ra147.

Thorp, B.C., and Badoux, X. (2018). Atrial fibrillation as a complication of ibrutinib therapy: clinical features and challenges of management. Leuk. Lymphoma *59*, 311–320.

Treon, S.P., Tripsas, C.K., Meid, K., Warren, D., Varma, G., Green, R., Argyropoulos, K.V., Yang, G., Cao, Y., Xu, L., et al. (2015). Ibrutinib in previously treated Waldenstrom's macroglobulinemia. N. Engl. J. Med. *372*, 1430–1440.

van den Berg, C.W., Okawa, S., Chuva de Sousa Lopes, S.M., van Iperen, L., Passier, R., Braam, S.R., Tertoolen, L.G., del Sol, A., Davis, R.P., and Mummery, C.L. (2015). Transcriptome of human foetal heart compared with cardiomyocytes from pluripotent stem cells. Development *142*, 3231–3238.

Woyach, J.A., Smucker, K., Smith, L.L., Lozanski, A., Zhong, Y., Ruppert, A.S., Lucas, D., Williams, K., Zhao, W., Rassenti, L., et al. (2014). Prolonged lymphocytosis during ibrutinib therapy is associated with distinct molecular characteristics and does not indicate a suboptimal response to therapy. Blood *123*, 1810–1817.

Wu, J., Zhang, M., and Liu, D. (2016). Acalabrutinib (ACP-196): a selective second-generation BTK inhibitor. J. Hematol. Oncol. *9*, 21.

Yang, C., Al-Aama, J., Stojkovic, M., Keavney, B., Trafford, A., Lako, M., and Armstrong, L. (2015). Concise review: cardiac disease

modeling using induced pluripotent stem cells. Stem Cells *33*, 2643–2651.

Yeh, E.T., and Bickford, C.L. (2009). Cardiovascular complications of cancer therapy: incidence, pathogenesis, diagnosis, and management. J. Am. Coll. Cardiol. *53*, 2231–2247.

Zhang, Q., Jiang, J., Han, P., Yuan, Q., Zhang, J., Zhang, X., Xu, Y., Cao, H., Meng, Q., Chen, L., et al. (2011). Direct differentiation of atrial and ventricular myocytes from human embryonic stem cells by alternating retinoid signals. Cell Res. *21*, 579–587.

Zhang, Y., Dedkov, E.I., Teplitsky, D., Weltman, N.Y., Pol, C.J., Rajagopalan, V., Lee, B., and Gerdes, A.M. (2013). Both hypothyroidism and hyperthyroidism increase atrial fibrillation inducibility in rats. Circ. Arrhythmia Electrophysiol. *6*, 952–959.